# The Wigner function in paraxial optics II. Optical diffraction pattern representation

C.J. Román-Moreno* and R. Ortega-Martínez**
*Laboratorio de Óptica Aplicada, Centro de Ciencias Aplicadas y Desarrollo Tecnológico, Universidad Nacional Autónoma de México, A. P. 70-186, México, D. F., 04510, México.*
*e-mail: *carlosr@aleph.cinstrum.unam.mx,*
***roberto@aleph.cinstrum.unam.mx*

C. Flores-Arvizo
*Centro de Bachillerato "Jesús Reyes Heroles", DGB-SEP, Progreso No. 23, Col. Axotla, Álvaro Obregón, México, D. F., 01030*
*e-mail: carlinflores@yahoo.com.mx*

Recibido el 31 de julio de 2002; aceptado el 22 de octubre de 2002

The Wigner distribution function is a tool to visualize a signal in the space-frequency domain. Moreover, it can be produced by purely optical means. We describe the Brenner-Lohmann optical setup with monochromatic light, which produces the Wigner function. A signal composed of rectangle functions (optically produced by slits) has a Wigner function with a "sand clock" form. We point out the strong oscillations of the Wigner function between two interfering components, which has been called the *smile function* of a "Schrödinger's cat" state. This bears interesting optical diffraction patterns in our figures.

*Keywords:* Wigner distribution function; Fourier optics.

La función de distribución de Wigner permite visualizar a una función en el dominio mixto espacio-frecuencia. Además, puede producirse con arreglos puramente ópticos. En este artículo se describe el arreglo óptico de Brenner-Lohmann iluminado con luz monocromática que produce la función de Wigner. Una señal compuesta por funciones rectángulo (producida ópticamente con rendijas) tiene una función de Wigner en forma de "reloj de arena". Es importante notar las fuertes oscilaciones de la función de Wigner de dos componentes que interfieren y que han sido llamadas la "función sonrisa" del estado de gato de Schrödinger y que genera patrones de difracción de gran interés.

*Descriptores:* Función de distribución de Wigner; óptica de Fourier.

PACS: 42.25.Hz; 42.30.kq

## 1. Introduction

Every signal —such as a music piece— can be described in at least four ways, shown in Fig 1. We may plot its air pressure profile $u(t)$ as a function of time $t$ (top left), or its temporal Fourier transform $\tilde{u}(\nu)$ (top right). Both descriptions are complete and equivalent, but useless for the performing musician. He needs to read which note, of frequency $\nu$, he must produce at each time $t$. The community of world musicians has converged on the representation of such signals by their musical score (bottom left). This score satisfies the musician but not necessarily the scientist [1, 2], because he knows that the uncertainty principle prevents him from specifying the monochromatic frequency at an instant of time. One needs a finite time interval to measure a small frequency range —for practical matters, at least a full cycle. Longer intervals improve the accuracy of the frequency measurement but degrade the sharpness of the time measurement. This conflict between the musician and the scientist is resolved by the Wigner function (bottom right).

The Wigner quasiprobability distribution function or Wigner function was originally applied for the understanding of quantum corrections in thermodynamical equilibrium [3]. Since then, it has come to be used extensively in quantum optics because it provides a clear interpretation of pure and mixed states in phase space [4–7]. Applications of the Wigner function to signal analysis in the space–momentum

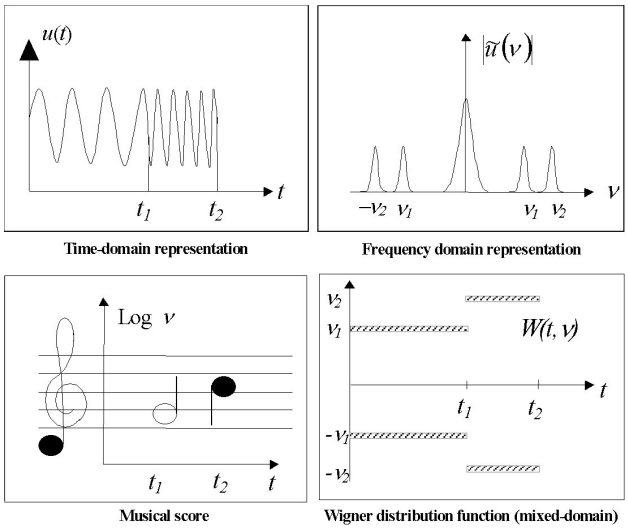


FIGURE 1. A time-dependent signal can be represented in several forms. This Figure shows an acoustical signal as a function of time (top-left) and as a function of frequency (top right). Musicians use the musical score, a time-frequency representation (bottom-left). The WDF is a mathematical mixed-domain completed representation.

and time–frequency domains are relatively recent and the new interpretation has been fruitful [8–11]. The Wigner function represents one-dimensional optical wave fields on the two-dimensional phase-space plane, by a height plot which is intuitively appealing and is rich in mathematical properties. In a recent paper, it was discussed with Zhao and ourselves the properties of the Wigner function that can be applied to optical lens systems related to this paper [12, 13].

We recall that the Wigner function of the signal $E(x)$ ($x \in \Re$, assumed to be square-integrable) is a function of the space and frequency domain ($x, k \in \Re$) defined by

$$W(x,k)=\int_{-\infty}^{\infty} dx' E(x+\tfrac{1}{2}x')E^*(x-\tfrac{1}{2}x')\exp(-ikx'), \quad (1)$$

or equivalently in the frequency domain, by

$$W(x,k)=\int_{-\infty}^{\infty} dk' \widetilde{E}(k+\tfrac{1}{2}k')\widetilde{E}^*(k-\tfrac{1}{2}k')\exp(ik'x), \quad (2)$$

where $E(x,k)$ and $\widetilde{E}(x,k)$ are a pair of Fourier transforms [1–13], where $\lambda$ is the wavelength and $k = 2\pi/\lambda$.

## 2. Experimental setup

To produce optically the Wigner function of some simple one-dimensional signals, we used the coherent-astigmatic processor proposed by Lohmann *et al*. in Ref. [1, 2], a major part of which is the sphero-cylindrical lens pair shown in Fig. 2. A coherent processor is an array consisting of a spatial filter and thin spherical lenses. When it is convenient to replace some spherical lenses by cylindrical lenses, the system is said to be an astigmatic processor. A powerful feature of coherently illuminated optical systems is that the Fourier transform of a signal exist in space. As a result, one can implement filtering operations directly in the Fourier domain. Spatial frequencies describe signals in space (such as images) in the same way that temporal frequencies describe signals in time.

To explain how Lohmann's apparatus works, we follow Goodman [14] in a didactic and direct (simple) description way: a ray entering a thin lens at the point of space coordinates $(x, y)$ will exit approximately at the same point on the opposite face. A thin lens solely produces thus, a delay in the phase $\delta\phi(x, y)$, given by

$$\delta\phi(x,y) = kn\, d(x,y),$$

where $k$ is the propagation number of the optical field, and $n$ and $d(x, y)$ are the index of refraction and the width of the lens at $(x, y)$, respectively. The effect of a thin lens is thus the multiplicative phase transform

$$t_l(x,y) = \exp[ik(d_0 + (n-1)d(x,y))], \quad (3)$$

where $d_0 = d(0, 0)$ is the width of the 'thin' lens on the optical axis. Hence, if $E(x, y)$ is the optical field distribution on the plane just before the lens, then the optical field on the plane immediately after the lens is given by

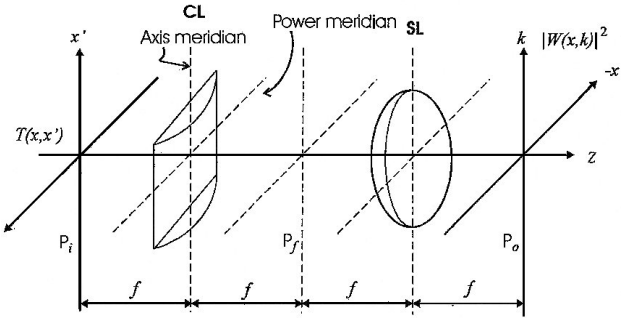


FIGURE 2. A coherent astigmatic optical processor (sphero-cylindrical) lens pair. An input transparency is on the front focal plane $P_i$ of the cylindrical lens. This lens produces the Fourier-transform on its back focal plane $P_f$ along its power meridian direction. The, a spherical lens produces another Fourier-transform operation on its back-focal plane $P_o$ resulting in an inverted image of the input transparency along the power meridian direction $(-x)$ and the Fourier-transform along the axis meridian direction $(k)$.

$$E'(x,y) = E(x,y)\exp[ik(d_0 + (n-1)\, d(x,y))]. \quad (4)$$

We follow here the common convention where rays propagate from left to right, and the radius of curvature is counted positive when the lens surface is convex, and negative when it is concave. In the paraxial approximation, one considers only the quadratic terms in the Taylor expansion of the surface function, that is, $d(x,y)-d_0 \approx g_{xx}x^2+2g_{xy}xy+g_{yy}y^2$. Unless otherwise specified, we imply that the lenses are spherical ($g_{xx} = g_{yy}$, $g_{xy} = 0$); when astigmatic, such quadratic surfaces can be brought always to principal axes by means of a rotation of the lens around the optical axis, or replaced by a spherical and a cylindrical lens in contact. So, when $R_1 > 0$ and $R_2 < 0$ are the radii of curvature of the first and second surfaces of the lens, respectively; then the width of the lens at all other points is approximated by

$$d(x,y) = d_0 - \left(\frac{1}{R_1} - \frac{1}{R_2}\right)\left(\frac{x^2+y^2}{2}\right). \quad (5)$$

In the paraxial approximation therefore, (4) yields the lens transformation

$$E'(x,y) = E(x,y)\exp\left[ik\left(nd_0 - \frac{1}{2f}(x^2+y^2)\right)\right], \quad (6)$$

where an important parameter of the lens is the *focal length* $f$, defined by

$$\frac{1}{f} = (n-1)\left(\frac{1}{R_1} - \frac{1}{R_2}\right). \quad (7)$$

The pupil function $P(x, y)$ for a lens of diameter $D$, is

$$P(x,y) = \begin{cases} 1, & x^2+y^2 \le (D/2)^2, \\ 0, & x^2+y^2 > (D/2)^2, \end{cases} \quad (8)$$

and accounts for the finite aperture of a real lens. The most remarkable property of converging lenses, *i.e.*, their ability

to perform a two-dimensional Fourier transform, stems from Fresnel's diffraction integral

$$E'(x',y') = \frac{e^{ikz}}{i\lambda z}\exp\frac{ik}{2z}\left(x'^2+y'^2\right) \times \iint_{-\infty}^{\infty} dx\,dy\,\left[P(x,y)\,E(x,y)\exp\frac{ik}{2z}\left(x^2+y^2\right)\right] \times \exp\frac{ik}{2z}\left(xx'+yy'\right). \quad (9)$$

Rearranging the integrals and exponents, one thus finds that a thin lens between two empty spaces will transform an object optical field $E(x,y)$ into an image field $E'(x',y')$, which is the convolution of the Fourier transform of the object field $\widetilde{E}(x',y')$ (generally, rescaled and multiplied by a quadratic phase with the Fourier transform of the pupil function). A spherical lens has the same focal length somewhere through its optical axis, hence it performs an isotropic Fourier transform. A cylindrical lens has infinite focal length in one plane, and can thus perform the Fourier transform only in the perpendicular direction.

Three distinct optical configurations have been used to perform the Fourier transform. (In all cases, one assumes that the illumination is monochromatic and that the distribution of light amplitude across the back focal plane of the lens is constant). In the first configuration, the object is placed directly on the lens surface; in the second, the object is placed at a distance $d$ in front the lens; and in the third case, the object is placed behind the lens, at a distance $d$ from the focal plane. Here we shall be concerned only with the more general geometry of the second case. So the object is at $d$ to the left of the lens, and it is illuminated by a normally incident field of amplitude $A$.

In the above paragraphs, we have discussed that a converging spherical lens produces, up to a phase factor, the Fourier-transform of a input transparency placed a distance $d$ in front of it; this Fourier-transform is on the focal plane of the lens. This Fourier-transform operation is due to the refracting power of the lens, so if we regard the optical field distribution only as a function of the spatial coordinate $x$, $E(x)$ on the input transparency plane, we get the Fourier-transform on the $k_x$ axis, which is parallel to the $x$-axis, on the focal plane.

A cylindrical lens has refracting power only along a plane perpendicular to its axis meridian. If we put a cylindrical lens with its axis (power meridian) perpendicular to the $x$-axis after a spherical lens, we get the Fourier-transform of the Fourier-transform of the input transparency, that is, the inverse image of the input transparency.

Because a cylindrical lens has no refracting power along its axis direction, it only introduces a change of phase on the $y$-axis, but the spherical lens produces the Fourier-transform along this direction. Finally, on the focal plane of the cylindrical lens we get the irradiance of the optical field distribution as a function of the space-coordinate $x$, and the wave number $k$ on the $y$-axis.

Paying attention to the definition of the Wigner function in Eq. (1), we see that Fresnel diffraction (9), while providing the Fourier transform of

$$F(x,y) = E(x+\tfrac{1}{2}y)\,E^*(x-\tfrac{1}{2}y), \quad (10)$$

will also provide the Wigner function of the signal $E(x)$. In case of real one-dimensional signals, the shifted product (10) can be produced in several ways. The one followed by us was to put two "identical" objects (generally two copies of a bar code transparency, but in our case a single slit, a pair of parallel slits, etc.), rotated one with respect to the other around the optical axis. The optical setup used in this paper was limited to one-dimensional signal. The rectangular slits were homogenously illuminated with a He-Ne laser, so a one-dimensional homogeneous optical field distribution along the horizontal axis is produced.

The square modulus of the Wigner function of a single slit, double slit and a triple slit and the "Schrödinger's cat" was obtained with the experimental array shown in Fig. 3,


FIGURE 3. A coherent astigmatic optical processor (Experimental setup). A slit is illuminated by a He-Ne laser beam. The sphero-cylindrical lens pair (SL-CL) produces the WDF of the optical -field leaving the slit- on the back-focal plane of the CL. The WDF is amplified by a microscope (MC) and recorded on a photographic film or by a CCD camera (not shown). The laser beam is spatial-filtered (SF), attenuated (AT) and collimated by a spherical lens (CSL) before goes through the slit.

where the slits and optical processor are located before a microscope. The single slit was described by a *rectangle* function given by

$$E(x) = \mathrm{rect}\left(\frac{x}{a}\right), \tag{11}$$

where the rect$(x)$ function is defined as usually by

$$\mathrm{rect}\,(x) \equiv \begin{cases} 1, & |x| < 1/2 \\ 1/2, & |x| = 1/2 \\ 0, & |x| > 1/4. \end{cases} \tag{12}$$

The WDF for the single slit is given by

$$W(x,k) = \frac{2\sin\left[k\left(-2|x|+a\right)\right]}{k}, \qquad |x| < a/2\,. \tag{13}$$

A counter-clockwise rotation of one slit around the beam propagation direction (see Fig. 4a and 4b) introduces a one-dimensional distribution along the $x'$ direction which made an angle $\theta$ with the $x$-axis, so that one-dimensional distribution along the $x-$ axis is given as

$$E(x' = x\cos\theta + y\sin\theta) = E(\cos\theta(x + y\tan\theta))$$

so, if $\theta = 26^0\,33'\,54.18$" then the optical field strength takes the form $E\left(0.8944\,(x + y/2)\right)$.

The double slit can be represented by the sum of two rectangular functions

$$E(x) = \mathrm{rect}\left(\frac{x - b/2}{a}\right) + \mathrm{rect}\left(\frac{x + b/2}{a}\right), \tag{14}$$

and the WDF for the double slit is

$$W(x,k;E) = \begin{cases} \dfrac{4}{k}\sin\left[k\left(-2|x|+a\right)\right]\cos\left(kb\right), & |x|<a/2 \\ \dfrac{2}{k}\sin\left[k\left(-2\left||x|-\frac{b}{2}\right|+a\right)\right], & |x-b/2|<a/2, \end{cases} \tag{15}$$

The triple-slit signal and its WDF can be represented, respectively, as

$$E(x)=\mathrm{rect}\left(\frac{x-b}{a}\right)+\mathrm{rect}\left(\frac{x}{a}\right)+\mathrm{rect}\left(\frac{x+b}{a}\right), \tag{16}$$

and

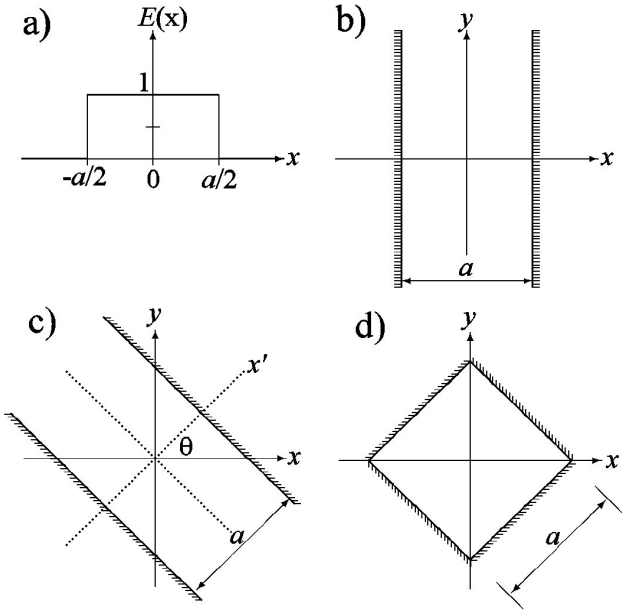


FIGURE 4.1 One slit (left). (a) A one-dimensional signal function $\overline{E}(x)$. (b) Two-dimensional wavefield function $E(x,y) = \overline{E}(x)$ on the object plane. (c) Function on the plane rotated counterclockwise by an angle of $\theta = 26^\circ 34'$ around the origin. (d) Product of two copies of $E(x,y)$ rotated by $\pm\theta$ is the object wave field $\overline{E}[a(x + (1/2)y)]\,\overline{E}[a(x - (1/2)y)]$ that will be Fourier transformed.

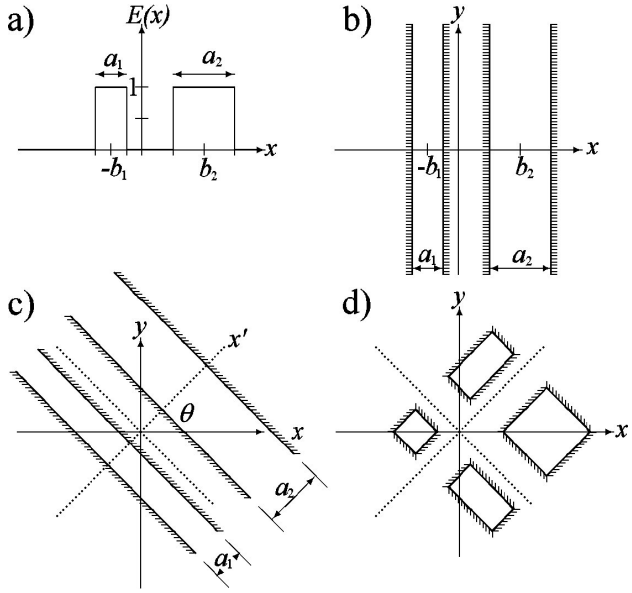


FIGURE 4.2 Two unequal slits (right). (a) A one-dimensional signal function $\overline{E}(x)$. (b) Two-dimensional wavefield function $E(x,y) = \overline{E}(x)$ on the object plane. (c) Function on the plane rotated counterclockwise by an angle of $\theta = 26^\circ 34'$ around the origin. (d) Product of two copies of $E(x,y)$ rotated by $\pm\theta$ is the object wave field $\overline{E}[a(x + (1/2)y)]\,\overline{E}[a(x - (1/2)y)]$ that will be Fourier transformed. and two unequal slits (right).

$$W(x,k;E)=\begin{cases}\dfrac{2}{k}\sin\left[k\left(-2|x|+a\right)\right]\left[2\cos(2kb)+1\right], & |x|<a/2\\ \dfrac{4}{k}\sin\left[k\left(-\left|2\left|x\right|-b\right|+a\right)\right]\cos(kb), & \left||x|-b/2\right|<a/2\\ \dfrac{2}{k}\sin\left[k\left(-2\left||x|-b\right|+a\right)\right], & \left||x|-b\right|<a/2\,.\end{cases} \tag{17}$$

## 3. Results

The rotation by angles $\pm\phi$ of the two copies of the bar-code signal $\overline{E}(x)$ give the fields $E(x,y)=\overline{E}(x\cos\phi\pm y\sin\phi)$ on the two-dimensional screen [1, 2, 15] (see Fig. 4). To obtain the shifts in Eq. (10) up to a common scale, it is thus required to rotate by the angle which fulfills $\sin\phi/\cos\phi=\pm1/2$, or $\phi=\pm\arctan\frac{1}{2}\approx 26°34'$. For simplicity, in our optical set up, we rotate the slits a $45^0$. This angle introduces a change in scale along the $x$-axis.

The functions that were mathematically considered are shown in Fig. 4a and 4b. The characteristic "sand clock" image is due to the sphero-cylindrical lens of the coherent processor and is shown in Fig. 5.

On Fig. 5 (top left), we can see the brightest sand clock-like" spot and some oscillations above and below it. These oscillations are much less intense than the central trace, but they can become visible easily on a photographic film. On Fig. 5 (top right) it is shown the square modulus of the WDF of a double slit. The trace on the extremes are produced by each slit and the one on the center is due to the interference of the two slits. It can be interpreted as a "optical Schrödinger's cat state". On the bottom of Fig. 5, it is shown the square modulus of the WDF of a triple slit. The first and fifth patterns (from left to right) are the square modulus of the WDF of the the first and third slits, respectively. The third pattern is a superposition of the the square modulus of the WDF of the second slit and the interference of the optical fields from the first and third slits. The second and fourth patterns are due to the interference of the fields from the first and second and the second and third slits, respectively. The nterference patterns alsp show several oscillatios (related to the "cat's smile fucntion").

A computer simulation was done using Eqs. (13), (15) and (17) to illustrate the utility of this representation and can be seen in Fig. 6 and 7. We bring attention to the fact that the region of strong oscillations in the Wigner function of the diffraction and interference patterns bears a lot of information that can be use for several applications like the characterization of ultrashort pulses, "chirp" measurements, holographic, laser spectroscopy and other applications [8–17].

## 4. Conclusions

In this paper, we have shown that the square modulus of WDF can be easily produced with a simple optical setup, where the sphero-cylindrical lens pair gives the images and the Fourier transfom of the slit, simultaneously. Also, the interference pattern of a multiple slit of a WDF can be associated to the"Scrödinger cat's smile". The experimental data and the

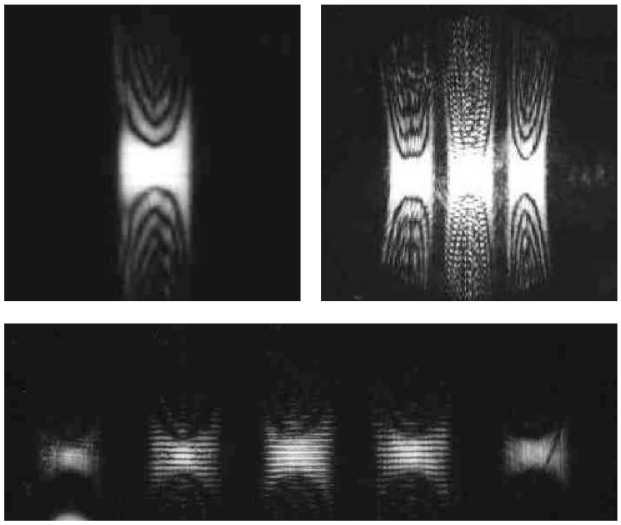

FIGURE 5. Square Modulus of the Wigner Function for a uniform illuminated single slit (top left), for a double slit (top right) and for a triple slit (bottom).

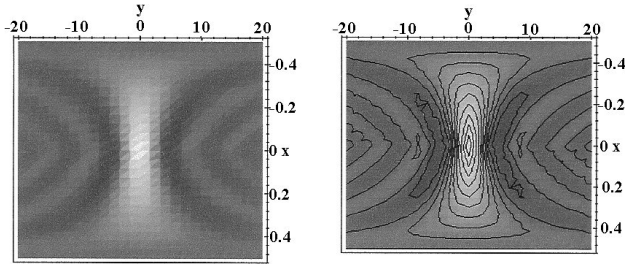


FIGURE 6. Plot of the square modulus of the Wigner Function for a uniform illuminated single slit.

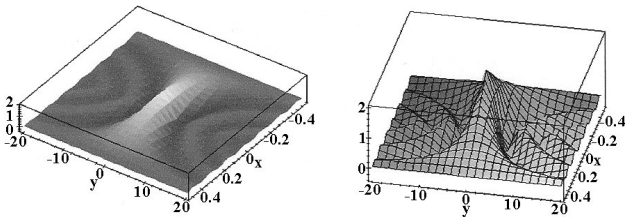


FIGURE 7. Plot of the square modulus of the Wigner Function of a single slit.

mathematical approach discussed here showed a good method to measure the distortion usually present in diffraction patterns, particularly interesting is the Wigner optical representation. This optical technique allows to illustrate quantum effects that are hardly shown with other methods.

On Fig. 5, the photographs clearly show the diffraction and interference patterns with the oscillations discussed in this paper. Fig. 6 and 7 are plots of the calculated WDF for a single slit. These plots are related to the pattern of single slit.

A close association between physical concepts and up-to-date optical techniques are found in the literature. Here, we present our efforts in this direction and a brief review of recent hot topics in the field of optics.

This presentation is our present work that we started at the laboratory, where students of electrical engineering and physics will be trained in these mathematical concepts, such as Fourier transform, cross and autocorrelation for ultrashort pulse characterization techniques, such as FROG, sonograms, time-frequency techniques and its vast applications in physical optics, dispersion, holography, nonlinear optics, telecommunications, tomography and ultrafast spectroscopy [18].

## Acknowledgements

We thank B. Wolf and A. García for their comments on the text an Ms H. Estrada for her assistance in preparing the text. We also thank A. A. Rodríguez for his help in preparation of the photographs. C. J. Roman and C. Flores had a support from Dirección General de Asuntos del Personal Académico-Universidad Nacional Autónoma de México(Project # 1N104597 and 1N108900) and Consejo Nacional de Ciencia y Tecnología (México)(Project # 4480-A9406 and 34921-E). R. Ortega is member of the *Sistema Nacional de Investigadores* (#6095).

1. H.O. Bartelt, K.H. Brenner, and A.W. Lohmann, *Opt. Commun.* **32** (1980) 32.
2. K.H. Brenner and A.W. Lohmann, *Opt. Commun.* **42** (1982) 310.
3. E. Wigner, *Phys. Rev.* **40** (1932) 749.
4. K.B. Wolf and A.L. Rivera, *Opt. Commun.* **144** (1997) 36.
5. K.B. Wolf, D. Mendlovic, and Z. Zalevsky, *Appl. Opt.* **37** (1998) 4374.
6. K.B. Wolf, M.A. Alonso, and G.W. Forbes, *J. Opt. Soc. Am. A* **16** (1999) 2476.
7. T. Alieva and M.J. Bastiaans, *J. Opt. Soc. Am. A* **17** (2000) 2319,
8. S. Mukamel, C. Ciordas-Ciurdariu, and V. Khidekel, *IEEE J. Quantum Electron.* **32** (1996) 1278.
9. L. Stanković, *IEEE Trans. Acoust. Speech, Signal Processing* **45** (1997) 543.
10. M.O. Scully, H. Lee, E. Gómez, and R. Ortega-Martínez, *Proc. of AIP XXXI ELAF* **CP464** (1999) 221.
11. R. Ortega-Martínez and C.J. Román-Moreno, *Recent Res. Devel. Optics* **1** (2001) 1.
12. D. Zhao, F. Ge, and S. Wang, *J. Mod. Opt.* **48** (2001) 2155.
13. R. Ortega-Martínez, C.J. Román-Moreno, and A.L. Rivera, *Rev. Mex. Fis.* **48** (6)(2002) 565.
14. J.W. Goodman, *Introduction to Fourier Optics*(McGraw-Hill, Singapore, 1996).
15. R.J. Marks II, J.F. Walkup, and T.F. Krile, *Appl. Opt.* **16** (1977) 746.
16. R. Trebino, K.W. DeLong, D.N. Fittinghof, J.N. Sweetzer, M.A. Krumbügel, B.A. Richman, and D.J. Kane, *Rev. Sci. Instrum.* **68** (1997) 3277.
17. R. Ortega-Martínez, C.J. Román-Moreno, and D. Kouznetsov, *J. Mod. Opt.* **46** (1999) 2069.
18. I.G. Cormack, W. Sibbett, R. Ortega-Martínez, and D.T. Reid, *Rev. Sci. Instrum.* **72** (2001) 4071.